JJEES

JJEES (2024) 15 (2): 82-93
ISSN 1995-6681

Jordan Journal of Earth and Environmental Sciences

Black Carbon Concentration in the District of Ar-Ramtha, Northern Jordan, and its Sources at Seven Wavelengths

Abdallah M. Mallak[1], Khadeejeh M. Hamasha[1*], Manal J. Abdallah[1]

[1]Physics Department, Yarmouk University, Jordan

Received March 1, 2023; Accepted September 13, 2023

Abstract

Variations of black carbon concentration and its sources identification were studied in Ar-Ramtha District , north of Jordan, using the aetlalometer model AE33. Measurements at six sites showed that the black carbon concentrations almost have the same behavior due to the uniform nature of the region. The average value of the black carbon concentration in the six sites was 1778 ng/m^3, 2288 ng/m^3, 1605 ng/m^3, 1785 ng/m^3, 2267 ng/m^3, and 2606 ng/m^3 respectively. Analysis of the measurements and Angstrom exponents, pre-calibrated in the instrument, revealed the ability of these variations to apportion black carbon from its sources. The largest contribution of black carbon was from fossil fuels at all sites. The absorption coefficients for each wavelength were measured at all sites. For a wavelength of 370 nm, it was discovered that the absorption coefficient had a maximum value of 58. 27Mm-1 while it it was 20.25 Mm^{-1} at 880 nm. In all sites, the average absorption coefficients reached their highest value at a wavelength of 370 nm, demonstrating the inverse relationship between wavelength and absorption coefficient.

Keywords: Black carbon, Aethalometer AE33, Ar-Ramtha District, Absorption coefficient, Angstrom exponent, Fossil fuel

1. Introduction

Black carbon (BC) is one of the elements that contribute to global warming by absorbing light from the atmosphere. It makes a significant contribution to global warming processes since it can influence local clouds and precipitation patterns (Abu Sada et al. 2015). As a result, its contribution to climate warming is on par with that of carbon dioxide (Bond et al., 2013). Because of its diminutive size that is less than 2.5 μm in diameter and ease of body penetration, BC has a detrimental effect on human health because it is the cause of numerous respiratory disorders (Janssen et al., 2012; Wang et al., 2017; Wang et al., 2021). In addition, these fine particles depend on the variability of weather parameters (Ali-Saleh et al., 2019, Al-Qinna 2018). In addition, due to its capacity to absorb nutrients crucial to plant growth, black carbon also has an impact on soil fertility (Glaser and Bruno, 2007).

Black carbon has been the subject of several recent studies in Jordan (Hamasha and Arnott 2009; Hamasha et al. 2010). Over the past 20 years, black carbon in Jordan has been increasing continuously, according to a recent research utilizing satellite data (Hamasha 2021). The main sources of black carbon in Jordan include transportation, industrial activity, and residential combustion activities such as cooking and heating. These findings highlight the need for effective legislation and regulations that will reduce Jordan's black carbon emissions while also improving the air quality and nation's overall health. The aethalometer type AE33 (Figure 1) was used in this investigation to assess the amount of black carbon and its sources (Fialho et al., 2005; Healy et al., 2017; Lack et al., 2013; Lu et al., 2015; Saleh et al., 2014) in the Ar-Ramatha region.

Figure 1. The Aethalometer AE33 in operation

2. Materials and Methods

In this study, measurements of BC were done in six different locations in Ar-Ramtha District. Ar-Ramtha District is located in the north of Jordan, near the Syrian-Jordanian border, opposite the Syrian city of Dar'a (Figure 2). It has an area of 485 km^2. The climate of Ar-Ramtha District is relatively dry. Due to its location on the verge of a desert area, it has a climate more like to that of the desert or a continental region, with hot, dry summers and rainy winters. Around 150–200 millimeters of precipitation fall annually in the eastern region, compared to 250–350

* Corresponding author e-mail: khamasha@yu.edu.jo

mm in the western and northern parts. The average daily temperature in summer is 25 degrees Celsius. Since 2011, Syrian refugees have a wide range of complex effects on Ar-Ramtha's surroundings. Land use, trash management, energy use, and water resources have been all impacted. Ar-Ramtha's expanding population has led to an increase in energy consumption. Due to increasing air pollution and greenhouse gas emissions, providing electricity to migrants via generators and other energy sources potentially harmful to the environment. The arrival of refugees in Ar-Ramtha has also led to a more demand in housing and infrastructure needs, which could endanger ecosystems and natural habitats. As a result, local ecosystem services and biodiversity may suffer.

Figure 2. A map of Jordan showing the location of the district of Ar-Ramtha in northern Jordan.

Measurements of BC were done using Aethalometer AE33. According to Virkkula et al. (2007), the equipment used in the measuring process attenuates light by depositing black carbon on the filter tape. The device supports DualSpot technology by simultaneously examining the light absorption by the deposits gathered at two parallel locations on the filter tape at varying loading rates (Drinovec et al., 2015). The Aethalometer AE33 is a device that measures the light absorption on a filter that has particles in it to estimate the amount of black carbon in the air in the present moment. The AE33 can provide accurate results in as little as one-minute using DualSpot technology and multi-wavelength optical analysis. The air sample is drawn through the instrument's input using an external pump operating at 5 liters per minute. The sample is put twice onto the filter tape once it has entered the optical chamber, each time at a different speed. The instrument analyzes the sample optically by comparing the quantity of light that passes through two places with the sample to the amount of light that goes through a loaded section of the filter tape in the reference region at wavelengths of 370, 470, 520, 590, 660, 880, and 950 nm. A detector on the other side gauges the amount of light that is transferred. Since the instrument is characterized by accumulated deposition of the sample on the filter, calculating the concentration of black carbon depends on the change in light attenuation every minute (Figure 3).

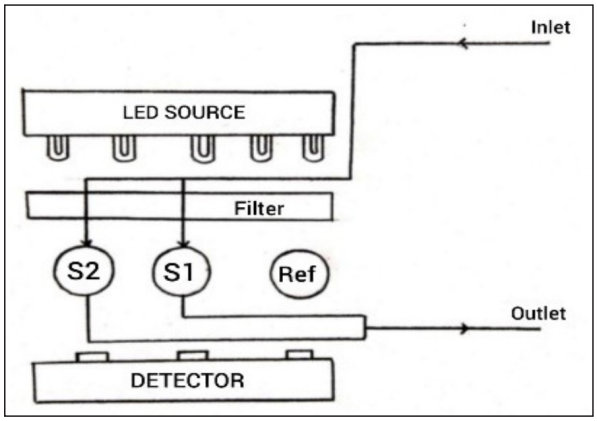

Figure 3. Schematic diagram of the optical analysis process of the sample on the filter.

The attenuation can be estimated using the signals. The detector reported using the formulas below:

$$\mathrm{ATN} = -100 \ln\left(\frac{I}{I_o}\right) \quad (1)$$

where the detector signals for the measurement location are I and the reference spot's detector signal is Io. The ratio, also known as the filter transmittance, reflects the amount of light that passes through the filter. In equation (1), the number 100 is included for convenience. The leakage factor () must be taken into consideration because the airflow is gauged after it goes through the filter. The optical chamber's lateral airflow is

$$F_{in} = F_{out} \times (1 - \zeta) \quad (2)$$

where F_{out} is the flow leaving the system after the filter, and F_{in} is the flow entering the input port. Consequently, the attenuation coefficient can be determined using

$$b_{atn} = S \times \frac{(\Delta ATN/100)}{F_{in}\Delta t} \quad (3)$$

where Δt is the time interval and S is the spot area.

The optical absorption of the filter deposits is impacted because the filter material scatters some of the incident light. According to Drinovec et al. (2015), factor C, which is dependent on the filter material, describes the amplification of optical absorption. The updated absorption factor b_{abs} is,

$$b_{abs} = \frac{b_{ATN}}{C} \quad (4)$$

The letter C (Weingartner et al. 2003) represents the multiple scattering parameter. Employing the relation, BC concentration is determined from the absorption coefficient.

$$BC = \frac{b_{abs}(\lambda)}{\sigma_{air}(\lambda)} \quad (5)$$

Where, σ is the mass absorption cross-section at wavelength λ. The values of σ at the seven wavelengths used in the AE33 observations are displayed in Table 1.

Table 1. Wavelength along with the cross-sectional area

λ (nm)	(m^2/g)
370	18.47
470	14.54
520	13.14
590	11.58
660	10.35
880	7.77
950	7.19

$$BC = \frac{BC_{measured}}{(1-k*ATN)} \quad (6)$$

where the compensating factor k is used. Seven wavelengths are tested simultaneously for optical absorption. The carbon black concentration is reported using data collected at an 880 nm wavelength. According to Sandradewi et al. (2008a, 2008b), the basis for source splitting of black carbon emissions is the wavelength dependence of the absorption coefficient. The optical absorption coefficient is the product of the absorption coefficient for burning biomass and the absorption coefficient for fossil fuels

$$b_{abs} = (b_{abs})_{ff} + (b_{abs})_{bb} \quad (7)$$

where, is the optical absorption parameter of the biomass burning, and (is the optical absorption parameter of the fossil fuels.

So,

$$BC = BC_{bb} + BC_{ff} = \frac{b_{abs}}{\sigma_{air(\lambda=880nm)}} \quad (8)$$

where, is BC of biomass burning source, and is BC of fossil fuels source. The equivalent black carbon produced by burning fossil fuels and biomass is thought to be well indicated by the absorption of near ultraviolet (UV) and infrared (IR) radiation, respectively. An important factor in identifying the origins of black carbon emissions is the optical absorption coefficient, which results from the burning of both biomass and fossil fuels. The AE33 model posits that emissions from burning fossil fuels and biomass follow spectrum dependences of λ^{-1} and λ^{-2} respectively. It is based on the difference in absorption coefficient wavelength dependence. The exponents that characterize the spectrum dependency are known as Angstrom exponents, and they are $\alpha_{ff} = 1$ for burning fossil fuels and $\alpha_{bb} = 2$ for burning biomass (Ran, L. et al. 2016).

Assessment of BC_{ff} and BC_{bb} contributions to the overall measured b_{abs} (λ) (component apportionment) is possible using the AE33 model,

$$b_{abs}(470nm) = b_{abs}(470nm)_{ff} + b_{abs}(470nm)_{bb} \quad (9)$$

$$b_{abs}(950nm) = b_{abs}(950nm)_{ff} + b_{abs}(950nm)_{bb} \quad (10)$$

In the source apportionment for AE33, the wavelength pairs 370 – 950 nm, 370-880 nm, 470-880 nm, and 470-950 nm were taken into account.

Biomass burning percentage BB (%) is:

$$BB(\%) = \frac{b_{abs}(950nm)_{bb}}{b_{abs}(950nm)} \quad (11)$$

The proportions of biomass burning and fossil fuels are then computed as follows:

$$BC_{bb} = BB \times BC \quad (12)$$

$$BC_{ff} = (1 - BB) \times BC \quad (13)$$

3. Results and Discussion

The field study was conducted in six different sites in Ar-Ramtha District to measure the black carbon concentrations using an Aethalometer AE33. Figure 4 shows the study areas in Ar-Ramtha District. The study regions were chosen based on the availability of various sources that contribute to the concentration of black carbon from burning fossil fuels and biomass. The data used in this study are from six separate days of measurements. Each measurement was conducted during all daytime.

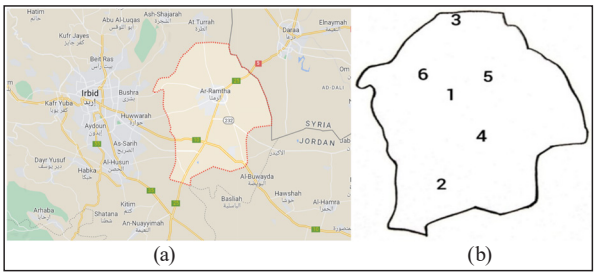

Figure 4. (a) The location of Ar-Ramtha District, north of Jordan, with respect to Irbid City and Syria boarder (b) the location of the study sites in Ar-Ramtha District

The study was conducted in the summer of 2021. The measurements were recorded by AE33 with a time resolution of one minute for a steady flow of aerosol samples (5 liters per minute). With the help of measured data from the instrument, this study examined the characteristics of the spatial and temporal patterns of black carbon to identify the origin of the BC concentration. The information utilized in this investigation is from measurements taken on six different days (Table 2). The six research sites in Ar-Ramtha District were carefully chosen in order to cover the entire region from north to south and from east to west. The southern region was chosen as the first location of Jordan University of Science and Technology (JUST), while the second site was selected in the north along the road going to Turrah . The third site was picked next to the Al-Shaqran station in the west and the fourth one was near Ar-Ramtha Government Hospital on the international route with Syria in the east. Additionally, an extremely crowded location was selected close to the Ar-Ramtha Health Center in the city center as the fifth site. The sixth location is near the Department of Licensing on the international route with Iraq in the district's southwest. Due to the limited availability and expensive cost of our aethalometer (AE33), we were unable to run the experiment simultaneously in all locations, so we did it over the course of several days. Because the locations are so close to one another and the local characteristics are the only ones that vary, it is reasonable to predict that the findings will be close. The most significant local factor is the crowdedness of the vehicles, which raises the level of atmospheric black carbon. Due to road closures at the time of the Corona pandemic, the inside routes are more congested with vehicles than the external ones.

Table 2. The study areas, date, area name, and properties.

Site #	Date	Area name	Properties
1	28/06/2021	Ar-Ramtha Comprehensive Health Center	The site is subject to the constant movement of vehicles and a populated area.
2	29/06/2021	The campus of the Jordan University of Science and Technology	The site is empty of students and has green cover
3	05/07/2021	Near the Northern Turrah Primary Health Center's	The site is subject to the constant movement of vehicles and a populated area.
4	07/07/2021	Near the Licensing Department	The site is on a public street, and it is highly subject to the constant movement of vehicles.
5	28/07/2021	Near Ar-Ramtha Government Hospital	The site is subject to the constant movement of vehicles, frequently populated, and surrounded by some cafes.
6	02/08/2021	Near the Al Shagran Gas Station	The site is on a public street, and it is highly subject to the constant movement of vehicles.

3.1. Variation of Black Carbon Concentration with Time

At each study site, the measurement represented the variance in the concentration of black carbon from burning biomass and fossil fuels (Figures 5 –10). Figure 5 shows that BC concentration in the first site varied between 772 ng/m^3 and 5177 ng/m^3. 92.94% of them were from fossil fuel sources.

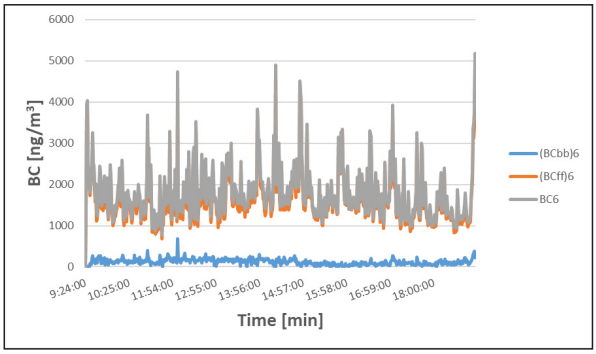

Figure 5. Variation of black carbon concentration from biomass burning and fossil fuel sources during the measurement in the first site on 28/06/2021

Figure 6 shows that BC concentration in the second site varied between 1002 ng/m^3 and 8030 ng/m^3. 89.65%of them were from fossil fuel sources.

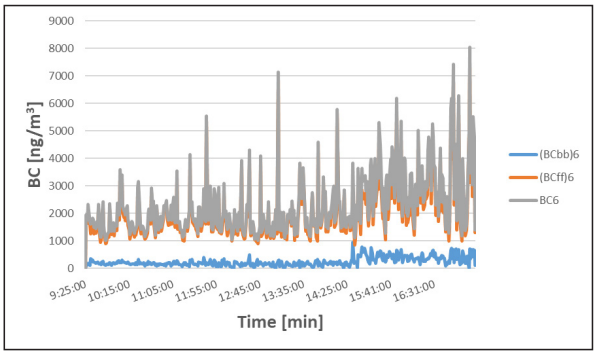

Figure 6. Variation of black carbon concentration from biomass burning and fossil fuel sources during the measurement in the second site on 29/06/2021

Figure 7 shows that BC concentration in the third site varied between 411ng/m^3 and 14299 ng/m^3.89.52% of them were from fossil fuel sources.

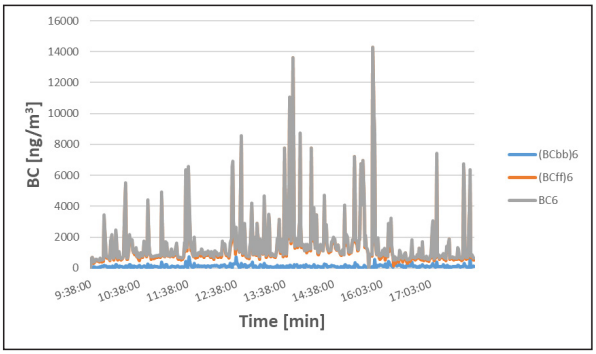

Figure 7. Variation of black carbon concentration from biomass burning and fossil fuel sources during the measurement in the third site on 05/07/2021

Figure 8 shows that BC concentration in the fourth site varied between 765 ng/m^3 and 9378 ng/m^3.95.15% of them were from fossil fuel sources.

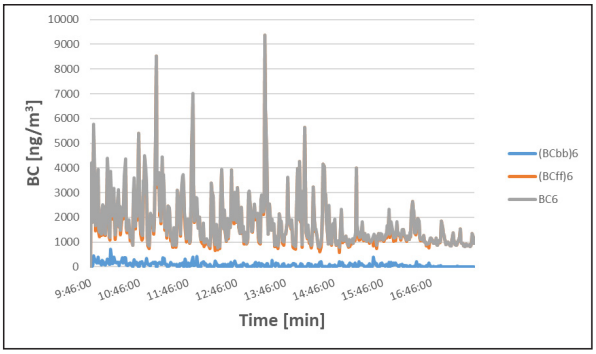

Figure 8. Variation of black carbon concentration from biomass burning and fossil fuel sources during the measurement in the fourth site on 07/07/2021

Figure 9 shows that BC concentration in the fifth site varied between 850 ng/m^3 and 8526 ng/m^3. 91.15% of them were from fossil fuel sources.

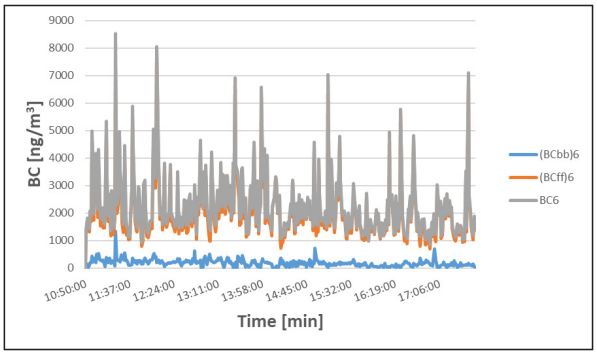

Figure 9. Variation of black carbon concentration from biomass burning and fossil fuel sources during the measurement in the fifth site on 28/07/2021

Figure 10 shows that BC concentration in the sixth site varied between 989 ng/m^3 and 16372 ng/m^3. 85.23% of them were from fossil fuel sources.

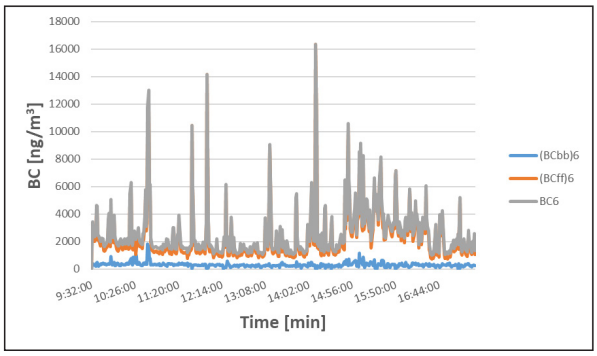

Figure 10. Variation of black carbon concentration from biomass burning and fossil fuel sources during the measurement in the sixth site on 02/08/2021

The average concentrations of BC during the measurements for all sites varied between 1605 ng/m^3 and 2606 ng/m^3. As seen in Figure 11, most the BC concentrations are from fossil fuel sources. This result is expected because the most sources of black carbon in Ar-Ramtha District were mobile transportation. The largest concentrations in BC were from site 6. It is very crowded with vehicles as it connects Ar-Ramtha area to Irbid via villages east of Irbid such as Sal and Bushra. The second largest concentration of black carbon was at site 2, the site of Jordan University of Science and Technology. Although, there were no students at the time of the measurements except for some staff who were on duty. Besides, it is very close to King Abdullah Hospital, which is very busy all the time. The result of BC concentration is very high and comparable to an urban area like Barranquilla, a Caribbean city in Colombia (Blanco-Donado et al. 2022).

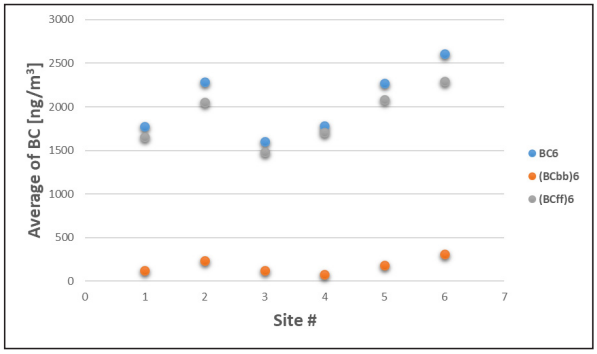

Figure 11. Average of black carbon concentration from biomass burning and fossil fuel sources during the measurement for all sites

3.2 Variation of Absorption Coefficients with Wavelengths

The absorption coefficients of the black carbon concentration from seven wavelengths were calculated based on the variation in the mass absorption cross-section of each wavelength during the measurement at each site. Figure 12 shows the time series of black carbon light absorption coefficients (b_{abs}) for the measurements at site 1 for the seven wavelengths (370nm, 470nm, 520nm, 590nm, 660nm, 880nm, and 950nm). The average b_{abs} of all wavelengths was 34.35 Mm^{-1}, 28.19 Mm^{-1}, 24.51 Mm^{-1}, 20.97 Mm^{-1}, 18.44 Mm^{-1}, 13.81 Mm^{-1}, and 13.05 Mm^{-1} respectively.

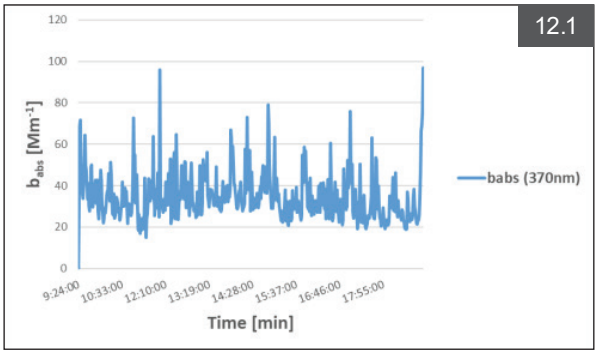

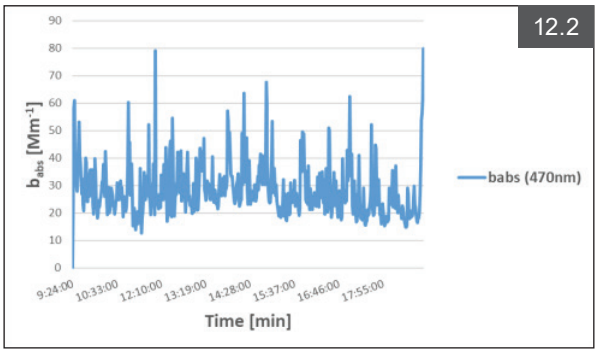

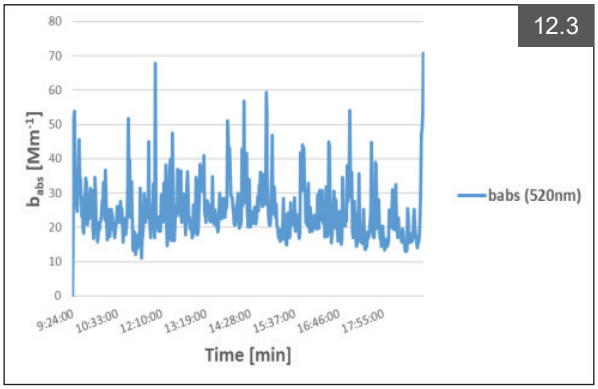

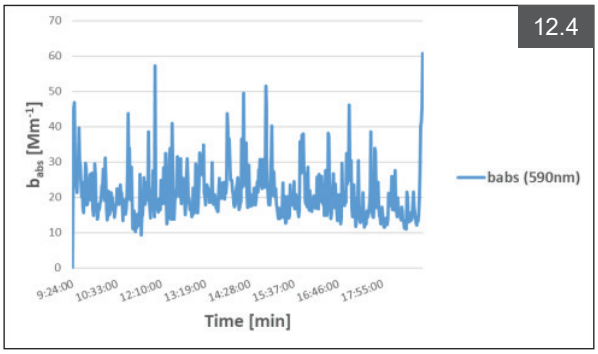

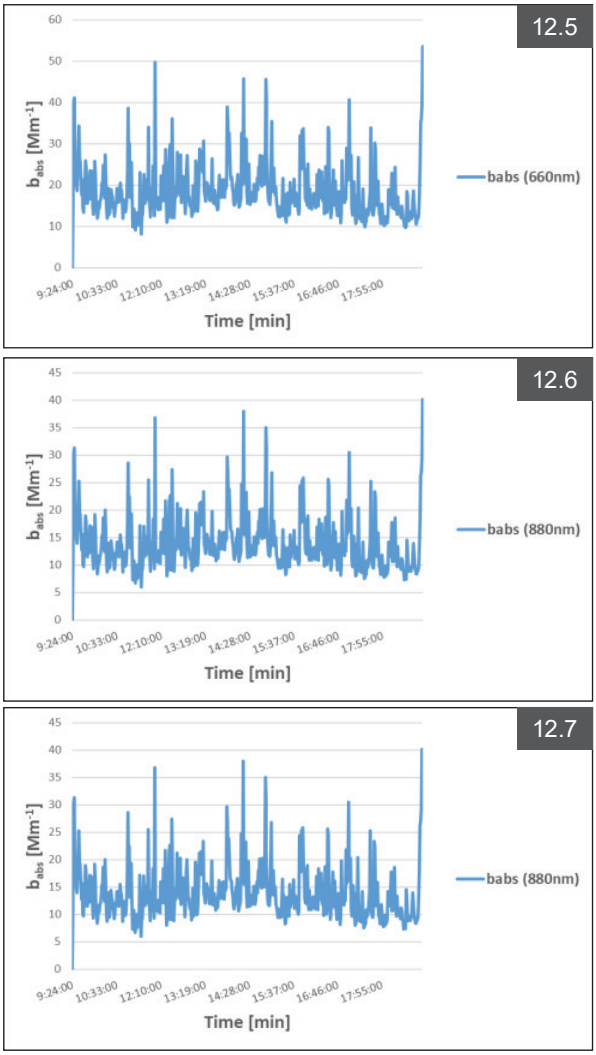

Figure 12. Variation in the absorption coefficients of black carbon during the measurement of the seven wavelengths in the first site on 28/06/2021

Figure 13 shows the time series of black carbon light absorption coefficients (b_{abs}) for the measurements at site 2 for the seven wavelengths (370nm, 470nm, 520nm, 590nm, 660nm, 880nm, and 950nm). The average b_{abs} of all wavelengths was 46.19 Mm^{-1}, 37.58 Mm^{-1}, 32.30 Mm^{-1}, 27.52 Mm^{-1}, 24.06 Mm^{-1}, 17.78 Mm^{-1}, and 16.82 Mm^{-1} respectively.

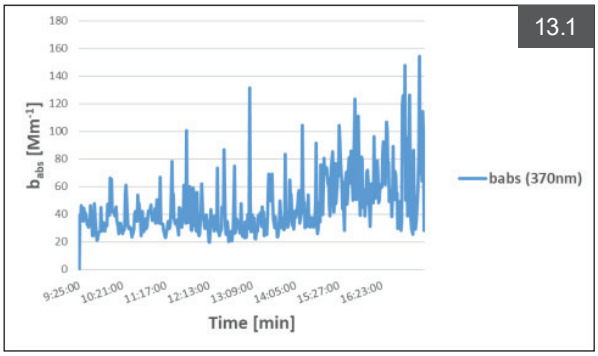

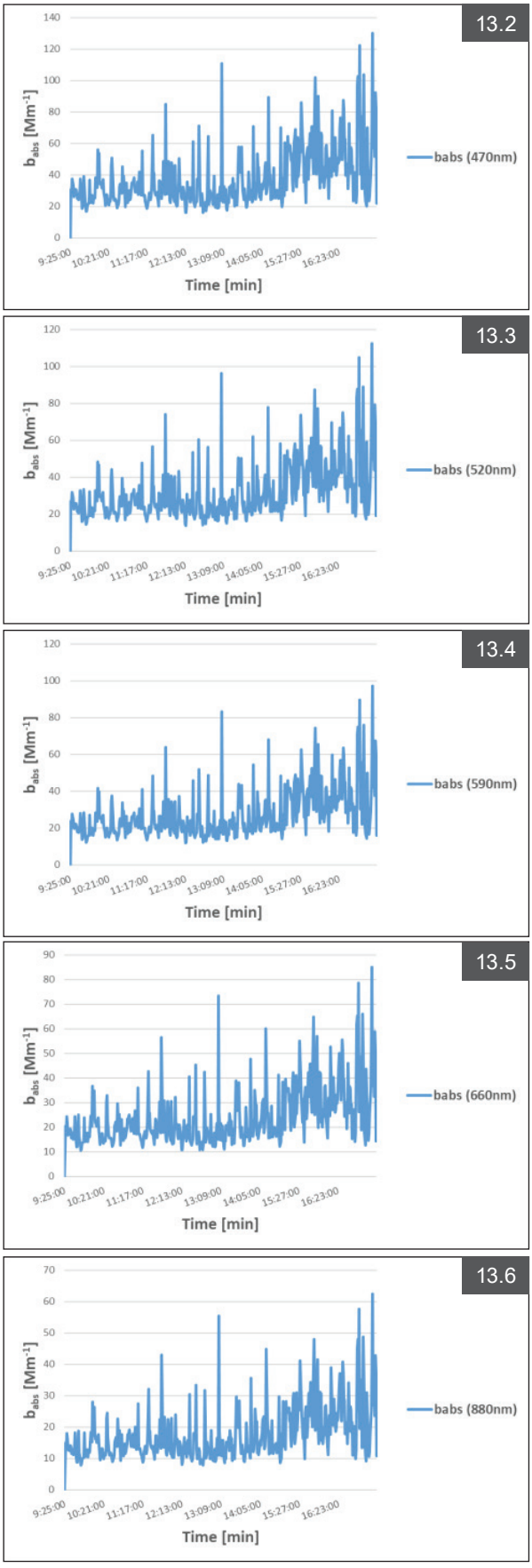

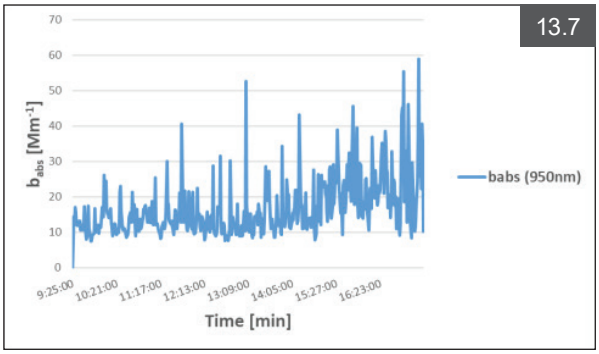

Figure 13. Variation in the absorption coefficients of black carbon during the measurement of the seven wavelengths in the second site on 29/06/2021

Figure 14 shows the time series of black carbon light absorption coefficients (b_{abs}) for the measurements at site 3 for the seven wavelengths (370nm, 470nm, 520nm, 590nm, 660nm, 880nm, and 950nm). The average b_{abs} of all wavelengths was 31.56 Mm^{-1}, 25.77 Mm^{-1}, 22.38 Mm^{-1}, 19.28 Mm^{-1}, 16.94 Mm^{-1}, 12.47 Mm^{-1}, and 11.93 Mm^{-1} respectively.

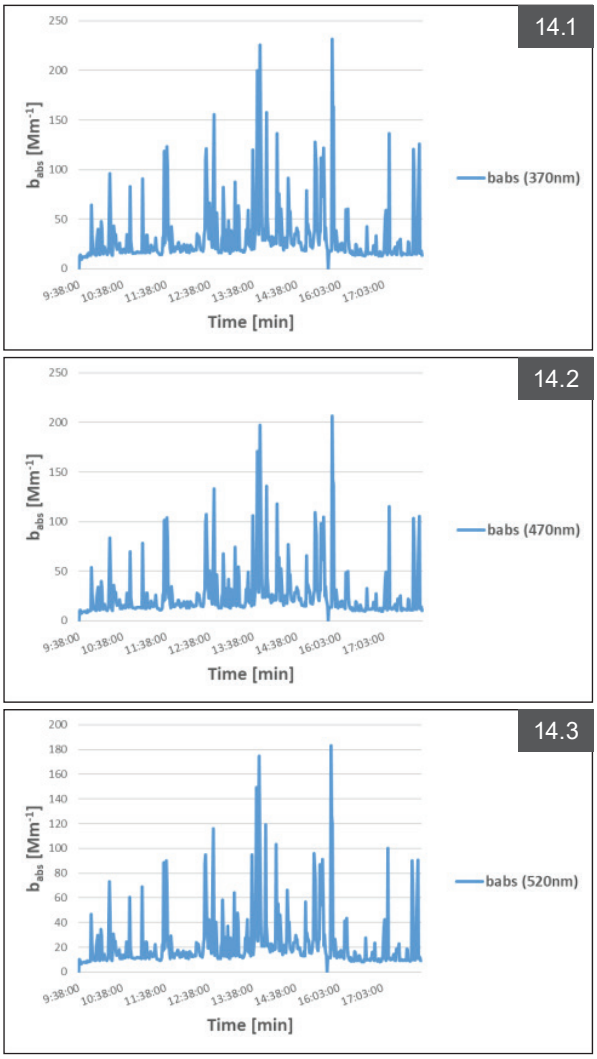

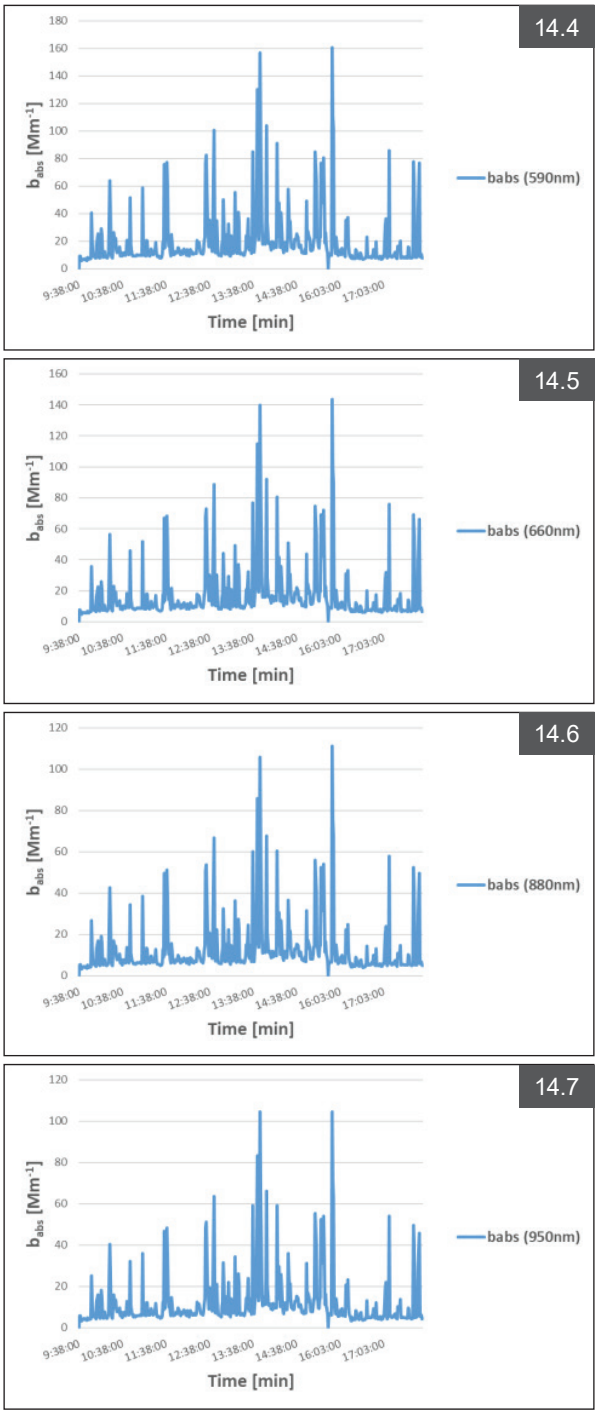

Figure 14. Variation in the absorption coefficients of black carbon during the measurement of the seven wavelengths in the third site on 05/07/2021

Figure 15 shows the time series of black carbon light absorption coefficients (b_{abs}) for the measurements at site 4 for the seven wavelengths (370nm, 470nm, 520nm, 590nm, 660nm, 880nm, and 950nm). The average b_{abs} for all wavelengths was 34.10 Mm^{-1}, 28.28 Mm^{-1}, 24.64 Mm^{-1}, 21.39 Mm^{-1}, 18.85 Mm^{-1}, 13.87 Mm^{-1}, and 13.52 Mm^{-1} respectively.

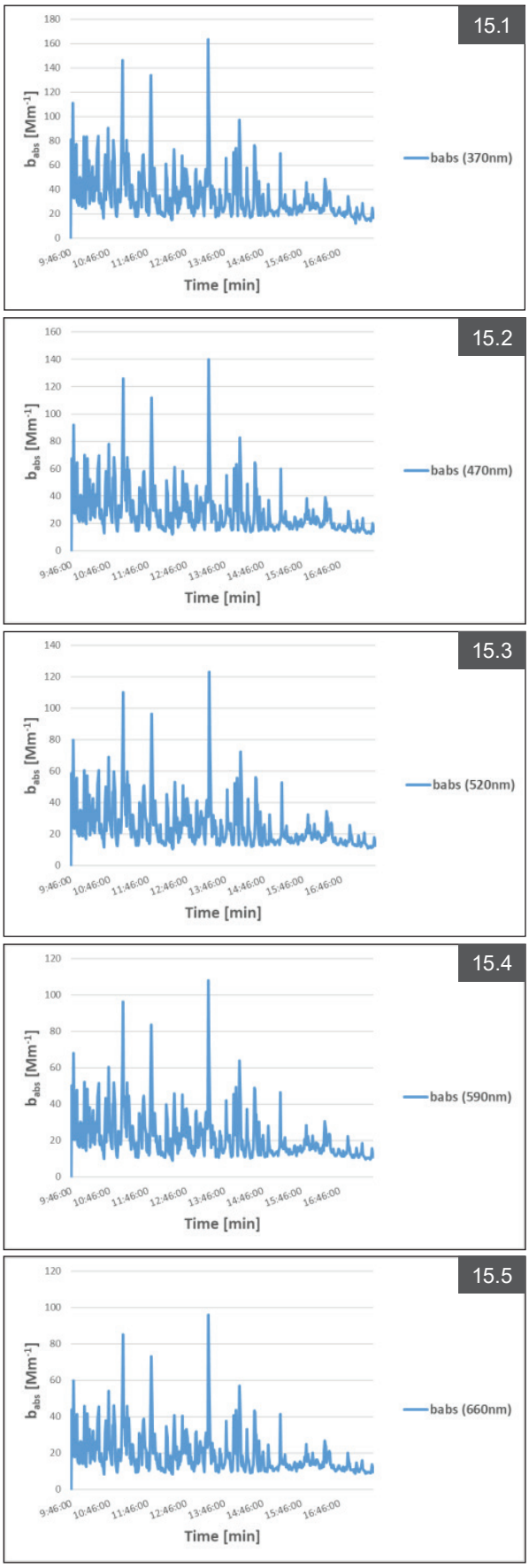

Figure 15. Variation in the absorption coefficients of black carbon during the measurement of the seven wavelengths in the fourth site on 07/07/2021

We note that the average values of the absorption coefficients of the seven wavelengths at sites 1 and 4 are identical. This similarlity indicates uniform nature of the two sites in terms of the availability of black carbon sources. Figure 16 shows the time series of black carbon light absorption coefficients (b_{abs}) for the measurements at site 5 for the seven wavelengths (370nm, 470nm, 520nm, 590nm, 660nm, 880nm, and 950nm). The average b_{abs} for all wavelengths was 44.29 Mm^{-1}, 36.24 Mm^{-1}, 31.37 Mm^{-1}, 26.93 Mm^{-1}, 23.57 Mm^{-1}, 17.61 Mm^{-1}, and 16.60 Mm^{-1} respectively.

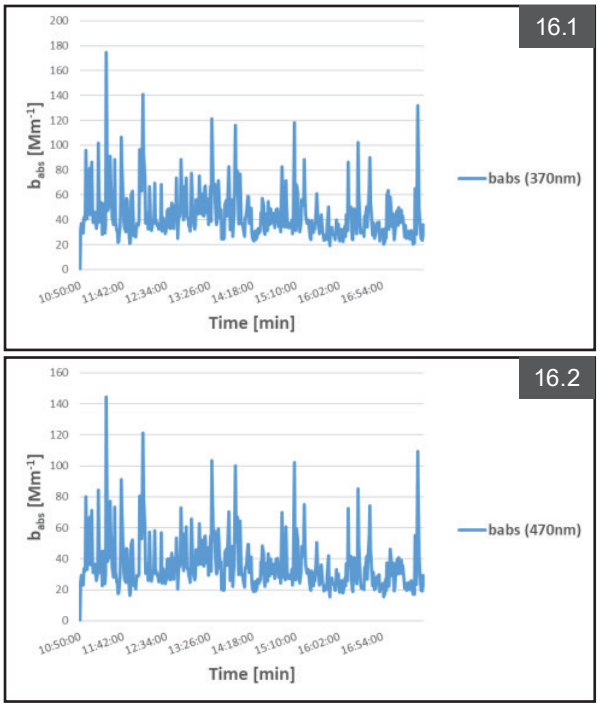

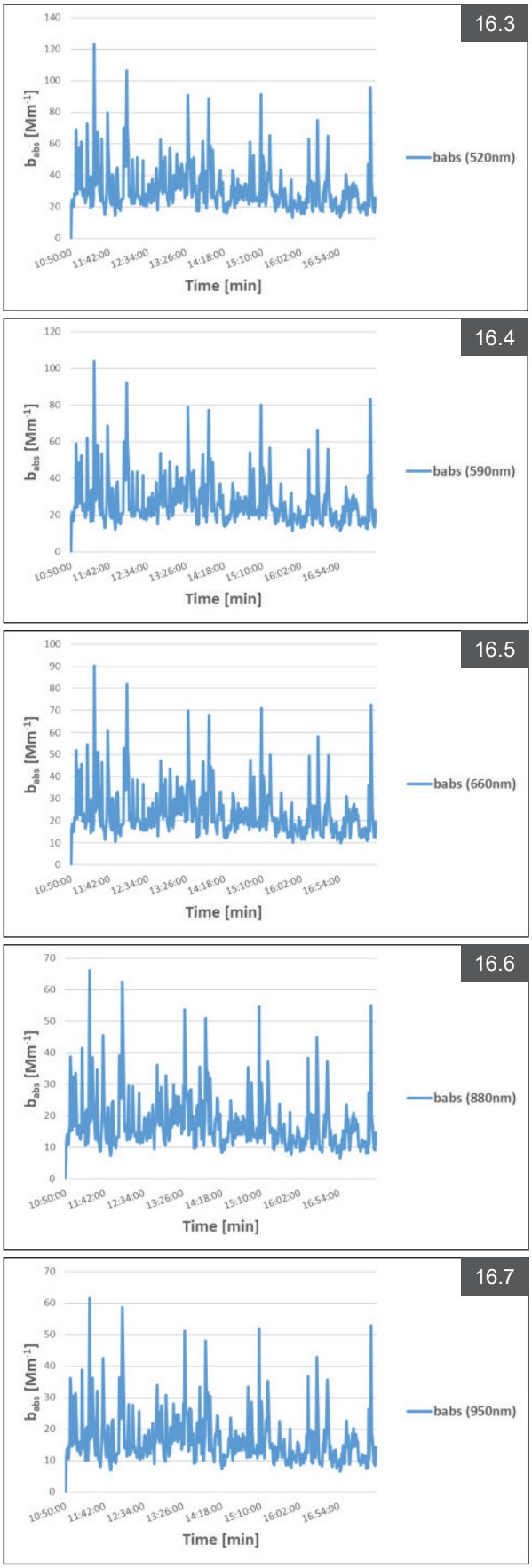

Figure 16. Variation in the absorption coefficients of black carbon during the measurement of the seven wavelengths in the fifth site on 28/07/2021

Figure 17 shows the time series of black carbon light absorption coefficients (b_{abs}) for the measurements at site 6 for the seven wavelengths (370nm, 470nm, 520nm, 590nm, 660nm, 880nm, and 950nm). The average b_{abs} for all wavelengths was 58.27 Mm^{-1}, 44.47 Mm^{-1}, 37.83 Mm^{-1}, 32.21 Mm^{-1}, 28.03 Mm^{-1}, 20.25 Mm^{-1}, and 19.66 Mm^{-1} respectively.

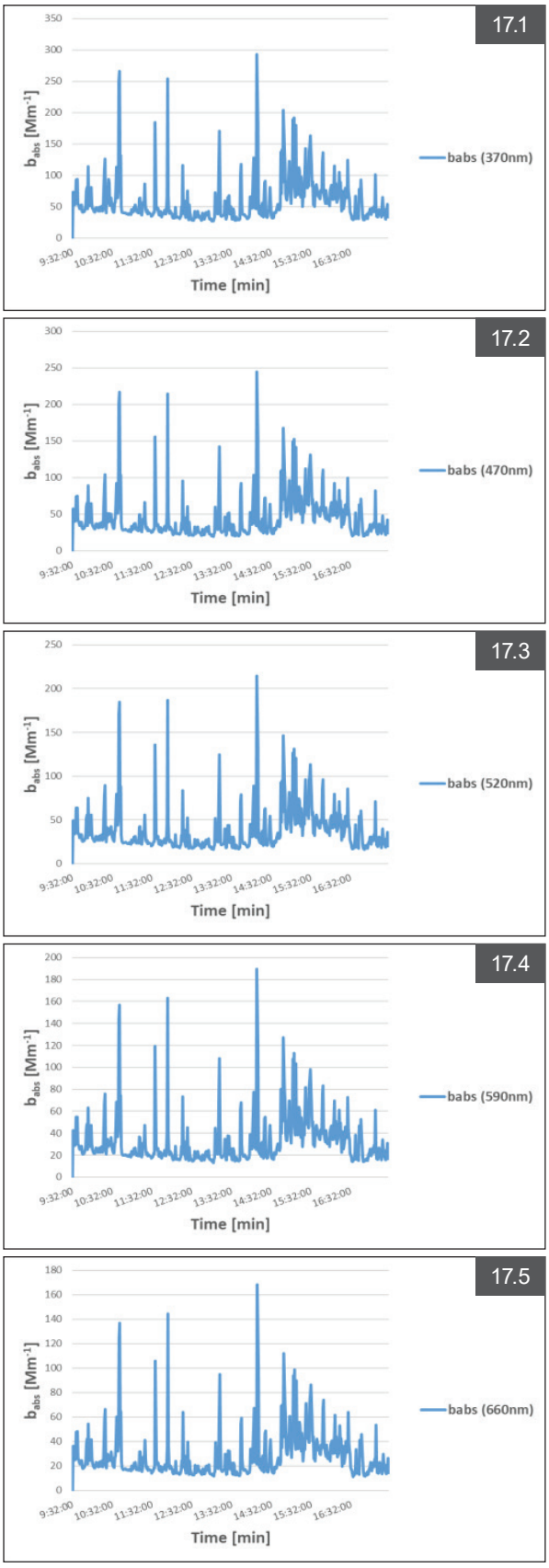

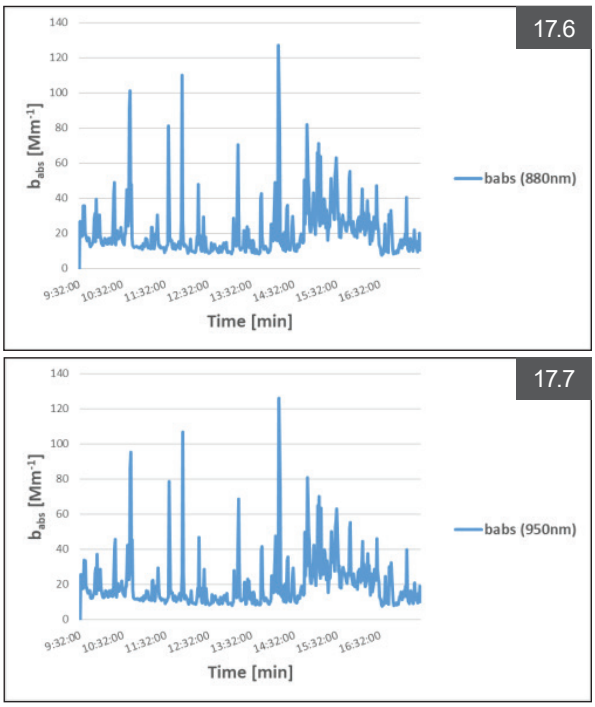

Figure 17. Variation in the absorption coefficients of black carbon during the measurement of the seven wavelengths in the sixth site on 02/08/2021

The average absorption coefficient values of the seven wavelengths were evaluated at six sites (Figure 18). It was found that the highest value was in site 6 because it is located on a public street, and it is subject to a greater degree of continuous movement of vehicles and population congestion than other sites. In addition, this site is considered the closest to the city of Irbid, which is considered one of the highest places in the concentration of black carbon in Jordan. It was found that the average values of the absorption coefficients in the six sites decreased with the increase of the wavelength because the absorption efficiency is proportional to the inverse of the wavelength. In addition, the values of the absorption coefficient at a defined wavelength are proportional to the size of the particles. This absorption process increases the air temperature and affects the climate because it removes energy from electromagnetic radiation and converts it into thermal radiation.

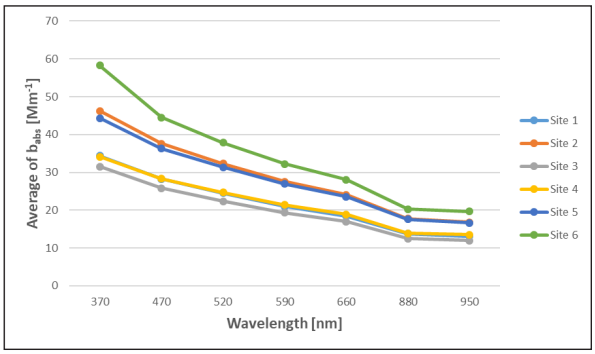

Figure 18. Average absorption coefficients of black carbon versus wavelength during measurements at different sites

Since the defining standard, used for reporting black carbon concentration, is at the wavelength of 880 nm, the average values of the absorption coefficients during the measurement campaign in Ar-Ramtha District were compared with a measurement in Irbid City, 20 km away from Ar-Ramtha. The average value of the absorption coefficient in Irbid City (Hamasha 2021) was (36.38Mm^{-1}) greater than in Ar-Ramtha District (15.96 Mm^{-1}). The reason is related to the combustion activities, population density, and overcrowded streets with buses and cars being more available in Irbid. In addition, it is related to the availability of cafes, shops, and restaurants that contribute to increasing the black carbon concentration. The measurement campaign in Ar-Ramtha was mostly in a less polluted, open, and less dense atmosphere population compared to the measurement campaign in Irbid.

Depending on the source, different BC concentrations have been discovered as having discernible effects on global warming. Even little increases in BC concentrations, according to reports, can have a big impact on the environment and people's health. The recommended yearly average limit for $PM_{2.5}$ (particulate matter with a diameter of less than 2.5 micrometers), as stated by the World Health Organization (WHO), is 10 g/m^3. Since black carbon is part of $PM_{2.5}$, lowering $PM_{2.5}$ concentrations can also aid in lowering black carbon emissions. The United Nations Framework Convention on climate change has developed rules and procedures for calculating and disclosing black carbon emissions in terms of global limits and measurements. The Climate and Clean Air Coalition has also established goals for lowering black carbon emissions in a number of industries, including brick manufacturing, transportation, and home energy. Numerous national standards and laws also govern the measurement and management of black carbon emissions.

3.3 The Role of the Angstrom Exponents (α) in Determining the Source of Black Carbon

The absorption exponent gives insight into the source of black carbon formation (Andreae and Gelencser 2006, Bergstrom et al. 2007). The role of the Angstrom exponents was evaluated in determining the contribution to the concentration of black carbon from its different sources during the measurement at all sites. It was found that the value absorption exponent of the measurements for all sites fluctuates around the value 1, which indicates the role of fossil fuels as the main contributor to the black carbon concentration (Table 3).

Table 3. Daily average absorption Angstrom exponent

Site #	Average Angstrom exponent
1	1.097
2	1.141
3	1.138
4	1.051
5	1.119
6	1.196

As can be seen in Table 3, the change of Angstrom exponent during the measurements in all sites fluctuates around 1 and is an indication of the major contribution of fossil fuels to the black carbon concentration.

4. Conclusion

The concentration of black carbon, which has a significant role in the global warming process, changes in the atmosphere depending on the geographical location and availability of its sources and is also affected by weather factors. The aethalometer AE33 provides real-time determination of the black carbon sources and percentages. The average value of all 6 sites in Ar-Ramtha district was found to be 2055 ng/m^3or 2.06μg/m^3 which is comparable to measurements done in urban areas. Analysis of measurements and angstroms pre-calibrated in the instrument revealed the ability to split black carbon from its sources. It was found that the source of fossil fuels is the dominant source of black carbon in the Ar-Ramtha region. It was also found that the absorption coefficient is inversely proportional to the wavelength.

Acknowledgment

The authors would like to thank Scientific Research and Graduate Studies Deanship at Yarmouk University, Jordan for supporting this work with Grant No. 18/2019.

Conflict of Interests

The authors declare that there are no conflicts of interest regarding the publication of this paper.

References

Abu Sada, A., Abu-Allaban M., and Al-Malabeh A., (2015), Temporal and Spatial Analysis of Climate Change at Northern Jordanian Badia, Jordan Journal of Earth and Environmental Sciences, 7 (2), ISSN 1995-6681, p. 87 – 93

Ali-Saleh, S., Shilbayeh Z., Alkattan H., Al-Refie M., Jaghbeir O., and Hussein T., (2019), Temporal Variations of Submicron Particle Number Concentrations at an Urban Background Site in Amman-Jordan, Jordan Journal of Earth and Environmental Sciences, 10 (1): ISSN 1995-6681, p. 7-14

Al-Qinna, M., (2018), Analyses of Climate Variability in Jordan using Topographic Auxiliary Variables by the Cokriging Technique, Jordan Journal of Earth and Environmental Sciences . 9 (1), ISSN 1995-6681, p. 67 - 74

Andreae, M. O. and Gelencsér, A.,(2006), Black carbon or brown carbon? The nature of light-absorbing carbonaceous aerosols, Atmos. Chem. Phys., 6, 3131–3148, https: // doi. org/ 10.5194/ acp-6-3131-2006.

Bergstrom, R. W., Pilewskie, P., Russell, P. B., Redemann, J., Bond, T. C., Quinn, P. K., and Sierau, B., (2007), Spectral absorption properties of atmospheric aerosols, Atmos. Chem. Phys., 7, 5937–5943 https://doi.org/10.5194/acp-7-5937-2007.

Blanco-Donado E.P., Schneider I.L., Artaxo P., Lozano-Osorio J., Portz L., Oliveira M.L.S., (2022), Source identification and global implications of black carbon, Geoscience Frontiers, 13 (1) , art. no. 101149

Bond, T. C., Doherty, S. J., Fahey, D. W., Forster, P. M., Berntsen, T., DeAngelo, B. J., Flanner, M. G., Ghan, S., Kärcher, B., Koch, D., Kinne, S., Kondo, Y., Quinn, P. K., Sarofim, M. C., Schultz, M. G., Schulz, M., Venkataraman, C., Zhang, H., Zhang, S., Bellouin, N., Guttikunda, S. K., Hopke, P. K., Jacobson, M. Z., Kaiser, J. W., Klimont, Z., Lohmann, U., Schwarz, J. P., Shindell, D., Storelvmo, T., Warren, S. G., and Zender, C. S., (2013), 715 Bounding the role of black carbon in the climate system: A scientific assessment, J. Geophys. Res., 118, 5380–5552, https://doi.org/10.1002/jgrd.50171.

Drinovec, L., Gregorič, A., Zotter, P., Wolf, R., Bruns, E. A., Prévôt, A. S. H., Petit, J. E., Favez, O., Sciare, J., Arnold, I. J., (2017), The filter-loading effect by ambient aerosols in filter absorption photometers depends on the coating of the sampled particles. Atmos. Meas. Tech. 10, 1043–1059, doi: 10.5194/amt-10-1043-2017.

Drinovec, L., Močnik, G., Zotter, P., Prévôt, A., Ruckstuhl, C., Coz, E., Rupakheti, M., Sciare, J., Müller, T., and Wiedensohler, A., (2015), "The" dual-spot" Aethalometer: an improved measurement of aerosol black carbon with real-time loading compensation", Atmos. Meas. Tech., 8, 1965–1979, https://doi.org/10.5194/amt-8-1965-2015.

Fialho, P., Hansen, A. D. A., and Honrath, R. E., (2005), Absorption coefficients by aerosols in remote areas: a new approach to decouple dust and black carbon absorption coefficients using seven wavelength Aethalometer data, J. Aerosol Sci., 36, 267–282.

Glaser and Bruno, (2007), "Prehistorically modified soils of central Amazonia: a model for sustainable agriculture in the twenty-first Century", Philosophical Transactions of the Royal Society B: Biological Sciences. 362 (1478): 187–196.

Hamasha, K. M. and W. P., Arnott, (2009), "Photoacoustic measurements of black carbon light absorption coefficients in Irbid city, Jordan", Environ. Monit. Assess, Doi 10.1007 / s10661-009-1017-3

Hamasha, K. M., M. S. Almomani , M. Abu-Allaban and W. P. Arnott, (2010), Study of Black Carbon Levels in City Centers and Industrial Centers in Jordan, Jordan Journal of Physics, Vol. 3, No. 1, pp 1-8

Hamasha, K., (2021), The Increasing Trend of Black Carbon and Organic Carbon in Jordan during the Period of 2007 to 2018, Nature Environment and Pollution Technology Vol 20 , No. 3, pp. 955 – 972, doi.org/10.46488/NEPT.2021.v20i03.004

Hamasha, K., (2023), Measurement of Black Carbon Absorption Coefficients Using an Aethalometer and Their Association with Visibility, Nature Environment and Pollution Technology ,Vol 22, No. 2, pp 741 – 753, doi.org/ 10.46488 / NEPT.2023. v22i02.017

Healy, R.M., Wang, J.M., Sofowote, U., Su, Y., Debosz, J., Noble, M., Munoz, A., Jeong, C. H., Hilker, N., Evans, G. J., (2019), Black carbon in the Lower Fraser Valley, British Columbia: Impact of 2017 wildfires on local air quality and aerosol optical properties. Atmos. Environ. 2019, 217, 116976, doi:10.1016 / j.atmosenv.2019.116976.

Janssen, N. A. H., Gerlofs-Nijland, M. E., Lanki, T., Salonen, R. O., Cassee, F., Hoek, G., Fischer, P., Brunekreef, B., Krzyzanowski, M., (2012), "Health effects of black carbon", The WHO European Centre for Environment and Health, Bonn, Germany, World Health Organisation Regional Office for Europe, Copenhagen, Denmark.

Lack, D. A., Bahreini, R., Langridge, J. M., Gilman, J. B., and Middlebrook, A. M., (2013), Brown carbon absorption linked to organic mass tracers in biomass burning particles. Atmos. Chem. Phys., 13, 2415–2422, doi:10.5194/acp-13-2415-2013.

Lu, Z., Streets, D. G., Winijkul, E., Yan, F., Chen, Y., Bond, T. C., Feng, Y., Dubey, M. K., Liu, S., Pinto, J. P., and Carmichael G. R., (2015), Light Absorption Properties and Radiative Effects of Primary Organic Aerosol Emissions. Environ. Sci. Technol., 49, 4868–4877, doi:10.1021/acs.est.5b00211.

Ran, L., Z.Z. Deng, P.C. Wang, X. A. Xia, (2016), Black carbon and wavelength-dependent aerosol absorption in North China Plain based on two year aethalometermeasurement, Atmospheric Environment, Vol. 142, pp. 132-144, ISSN 1352-2310, doi.org/10.1016/j

Saleh, R., Robinson, E. S., Tkacik, D. S., Ahern, A. T., Liu, S., Aiken, A. C., Sullivan, R. C., Presto, A. A., Dubey, M. K., Yokelson, R. J., Donahue, N. M. and Robinson, A. L., (2014), Brownness of organics in aerosols from biomass burning linked to their black carbon content. Natural Geoscience, 7, 647–650,

doi:10.1038/NGEO2220.

Sandradewi, J., Prévôt, A. S. H., Szidat, S., Perron, N., Alfarra, M. R., Lanz, V. A., Weingartner, E., and Baltensperger, U., (2008a), Using aerosol light absorption measurements for the quantitative determination of wood burning and traffic emission contributions to particulate matter, Environ. Sci. Technol., 42, 3316–3323, doi:10.1021/es702253m.

Sandradewi, J., Prévôt, A. S. H., Weingartner, E., Schmidhauser, R., Gysel, M., and altensperger, U., (2008b), A study of wood burning and traffic aerosols in an Alpine valley using a multi-wavelength aethalometer, Atmos. Environ., 42, 101–112.

Virkkula, A., Mäkelä, T., Hillamo, R., Yli-Tuomi, T., Hirsikko, A., Hämeri, K., and Koponen, I. K., (2007), A simple procedure for correcting loading effects of Aethalometer data, J. Air Waste Manage.,57, 1214–1222, doi:10.3155/1047-3289.57.10.1214.

Wang, L., Bao, S., Liu, X., Wang, F., Zhang, J., Dang, P., Wang, F., Li, B., Lin, Y., (2021), Low-dose exposure to black carbon significantly increase lung injury of cadmium by promoting cellular apoptosis, Ecotoxicology and Environmental Safety , ttps://doi.org/10.1016/j. ecoenv. 2021. 112703, 2021

Wang, J., Huang, L. Wang, C. Chen, D. Yang, M. Jin, C. Bai, Y. Song, Urban particulate matter triggers lung inflammation via the ROS-MAPK-NF-kappaB signaling pathway, J. Thorac. Dis., 9 (11) (2017), pp. 4398-4412, 2017

Weingartner, E., Saathoff, H., Schnaiter, M., Streit, N., Bitnar, B., and Baltensperger, U., (2003), “Absorption of light by soot particles: determination of the absorption coefficient by means of aethalometers”, J. Aerosol Sci. 34, 1445-1463